Article ID: 1000-324X(2023)04-0469-08 **DOI:** 10.15541/jim20220591

Enhanced Degradation of Methyl Orange with $CoFe_2O_4$@Zeolite Catalyst as Peroxymonosulfate Activator: Performance and Mechanism

WANG Lei[1], LI Jianjun[1,2], NING Jun[3], HU Tianyu[1,2], WANG Hongyang[1], ZHANG Zhanqun[1], WU Linxin[1]

(1. School of Materials Science and Engineering, Anhui University of Science and Technology, Huainan 232001, China; 2. Institute of Environment-friendly Materials and Occupational Health, Anhui University of Science and Technology, Wuhu 241000, China; 3. Anhui Shuiyun Environmental Protection Co., Ltd., Wuhu 241000, China)

Abstract: $CoFe_2O_4$@zeolite (CFZ) was prepared by using a co-precipitation hydrothermal method and used for synthetic dyes degradation by activating peroxymonosulfate (PMS). Comprehensive characterizations suggest that $CoFe_2O_4$ nanoparticles composing porous shell layer is uniformly covered on Na-A zeolite. The specific surface area of CFZ is 107.06 m^2/g, three times that of the original zeolite. Since CFZ has a saturation magnetization of 29.0 $A·m^2·kg^{-1}$, it could be separated efficiently by magnetic separation. Catalytic degradation experiments indicate that the removal of methyl orange (MO) in the CFZ/PMS system is much higher than that using CFZ or PMS alone. Under the optimum condition ([MO]=50 mg/L, [PMS]=1.0 mmol/L, 0.2 g/L CFZ, pH 8 and T=25 ℃), MO removal efficiency is up to 97.1%. Effect of various factors, including pH, PMS and CFZ dosage, MO concentration and presence of coexisting anions, on the catalytic performance of CFZ is carefully studied. Reactive oxygen species quenching experiments suggest that $^1O_2$ and $O_2^{\bullet-}$ play a dominant role in the degradation process. CFZ shows excellent recycling performance that the MO removal is declined by only 2.4% after 5 cycles. Catalytic degradation mechanism of the CFZ/PMS system is explored in detail.

Key words: advanced oxidation processe; peroxymonosulfate activation; magnetic catalyst; $CoFe_2O_4$@Zeolite; reactive oxygen species; degradation

Environmental problems concerning water pollution has drawn much attention of scholars in recent years. One of the prominent sewage types is effluent containing synthetic dyes discharged from pharmaceutical, printing, food, paper, and textile industries. The synthetic dyes in water pose serious threat to animal lives and human health[1]. Therefore, it is of great significance to find an effective method to remove synthetic dyes, *e.g.* methyl orange (MO), from water. MO is a typical anionic dye that belongs to azo group. Owing to its sturdy molecular structure, MO is difficult to be degraded by conventional biochemical methods[2]. In recent decades, advanced oxidation processes (AOPs), such as Fenton oxidation, photocatalytic oxidation, ozone oxidation and peroxymonosulfate (PMS) oxidation, have gained widespread attention as an efficient approach to sewage treatment[3-6]. Owing to their strong oxidation and high removal efficiency, AOPs have been employed to treat industrial sewage and sludge with high concentration pollutant and refractory to biochemical degradation[6]. Various organics, including antibiotic, phenolic compound, surfactant and synthetic dyes, could be converted to CO_2, H_2O and other harmless inorganic products by applying these methods[7-8].

Among them, PMS-based advanced oxidation process has high reactivity, strong oxidation capacity and produces little secondary pollution[9]. Therefore, it has great potential for industrial application. The strong oxidation comes from the reactive oxygen species (ROS) generated during the catalytic reaction, including hydroxyl radical (•OH), superoxide radical ($O_2^{\bullet-}$), sulfate radical ($SO_4^{\bullet-}$) and singlet oxygen ($^1O_2$)[6]. To improve the oxidation performance of PMS, various catalysts, including metals, metal oxides and heterogeneous metal-based catalysts, have been

Received date: 2022-10-09; **Revised date:** 2022-11-27; **Published online:** 2022-12-30
Foundation item: Natural Science Foundation of Anhui Province (1908085ME127); Research Foundation of the Institute of Environment-friendly Materials and Occupational Health (Wuhu), Anhui University of Science and Technology (ALW2021YF11)
Biography: WANG Lei (1998–), male, Master candidate. E-mail: wangleidreamer@126.com
王 磊(1998–), 男, 硕士研究生. E-mail: wangleidreamer@126.com
Corresponding author: LI Jianjun, professor. E-mail: ljj.hero@126.com
李建军, 教授. E-mail: ljj.hero@126.com

studied[10-11]. Spinel ferrite ($MeFe_2O_4$, Me=Co, Ni, Mn, Cu and Zn, *etc*.), a heterogeneous metal-based catalyst, has attracted much attention recently, due to its excellent catalytic activity[7]. Among them, $CoFe_2O_4$ has good catalytic activity owing to the full utilization of the catalytic activity of both Fe and Co, and the synergistic interaction between them[7,11]. $CoFe_2O_4$/PMS system was used to oxidize various organic pollutants in aqueous solution, such as antibiotics, pesticides, synthetic dyes and surfactant, with a degradation rate more than 90%[7,12-14].

Since $CoFe_2O_4$ is ferromagnetic, it can be separated from water efficiently by magnetic separation, which not only improves the solid-liquid separation, but also facilitates the recovery of the catalyst. However, strong magnetism makes $CoFe_2O_4$ particles conductive to agglomerate, especially for the nanoscale, which greatly reduces their specific surface area so as to weaken the catalytic performance[15]. To address the problem, $CoFe_2O_4$ nanoparticles were supported on carriers. In order to increase the effective supporting amount of catalyst and enhance the structure stability of their composite, materials with high surface area were selected as carriers. The carrier material is also required to have high acid-base stability and thermal stability to adapt to the harsh chemical environment in the synthesis process and using process. Various materials, including silica, titanium dioxide, zirconia and graphene, were employed as catalyst carriers[16]. Zeolite, as a cheap and stable inorganic porous material, well meets the above requirements, so it could be one of the best candidates for catalyst carrier.

Herein, magnetic $CoFe_2O_4$@zeolite (CFZ) was prepared by a co-precipitation hydrothermal method. Contents of the study were included as follows: (I) CFZ was synthesized and characterized. (II) The degradation of MO in different systems was compared. (III) Influence factors on the degradation were investigated. (IV) Stability and reusability of the catalyst were tested. (V) The presence of different ROS was determined.

1 Experimental

1.1 Preparation of CFZ

Coal gangue obtained from Huainan, China, was chosen as the raw material to prepare zeolite. The typical silica alumina ratio of Na-A zeolite is 1.0–2.0. To meet the requirement, $Na_2SiO_3·9H_2O$ was used to adjust the ratio. The coal gangue was successively pulverized and sieved. Then an aluminosilicate precursor was obtained by calcining the coal gangue powder for 2 h at 750 ℃[17]. 5.5 g precursor and 1 g $Na_2SiO_3·9H_2O$ were dispersed in 30 mL deionized water, and stirred for 30 min, and then solution A was obtained. Next, 6.0 mmol $FeCl_3·6H_2O$ and 3.0 mmol $CoCl_2·6H_2O$ were dissolved into 25.0 mL deionized water. The mixture was slowly added into 25 mL NaOH solution (3 mol/L) heating in a water bath at 90 ℃, and continued heating for 5 min. Then solution B was obtained. Both solution A and B were transferred into a hydrothermal reaction bottle and reacted at 90 ℃ for 10 h. The obtained solid products were washed with deionized water and ethanol, then dried at 60 ℃ in vacuum for 6 h. After grinding, magnetic CFZ catalyst were obtained.

1.2 Dye degradation experiments

Degradation experiments were carried out in 250 mL beakers at room temperature. Before the reaction, reagents were added into 100 mL MO solution. Part of the supernatant was extracted every few minutes to measure its absorbance. The removal rate of MO can be calculated as follows:

$$R = (C_1 - C_0)/C_0 \times 100\% \quad (1)$$

Where, R, C_1 and C_0 are the removal rate, current concentration and initial concentration of MO, respectively.

In the study, the effects of dosage of CFZ and PMS, solution pH, MO concentration, as well as common coexisting anions on the degradation were investigated. In addition, the stability and reusability of CFZ was tested. In the end, the contributed ROS in the CFZ/PMS system was determined.

Experimental details are described in the supporting materials.

2 Results and discussion

2.1 Characterization of the catalysts

X-ray diffraction (XRD) patterns of the zeolite, $CoFe_2O_4$ and CFZ are exhibited in Fig. 1(a). It can be seen that the diffraction peaks of CFZ all correspond to zeolite and $CoFe_2O_4$. The peaks at 2θ = 12.4°, 16.1°, 20.3°, 23.9°, 27.1°, 33.3°, 40.1°, 56.3° and 68.5° are attributed to the (111), (210), (220), (311), (321), (421), (521), (722) and (900) crystal plane diffraction peaks of Na-A zeolite (PDF#38-0214), separately. While the characteristic diffraction peaks located at 2θ = 18.3°, 30.1°, 35.4°, 37.1°, 43.1°, 53.4°, 57.0°, 62.6° and 74.0° correspond to the (111), (220), (311), (222), (400), (422), (511), (440) and (533) plane diffraction of $CoFe_2O_4$ (PDF#22-1086), respectively. There are no miscellaneous peaks in the diffraction patterns, indicating that CFZ is a composite material containing $CoFe_2O_4$ and Na-A zeolite. Since $CoFe_2O_4$ is ferromagnetic, CFZ has magnetism. As illustrated in the hysteresis loops (Fig. 1(b)), the saturation magnetization of CFZ is 29.0 $A·m^2·kg^{-1}$. Although this

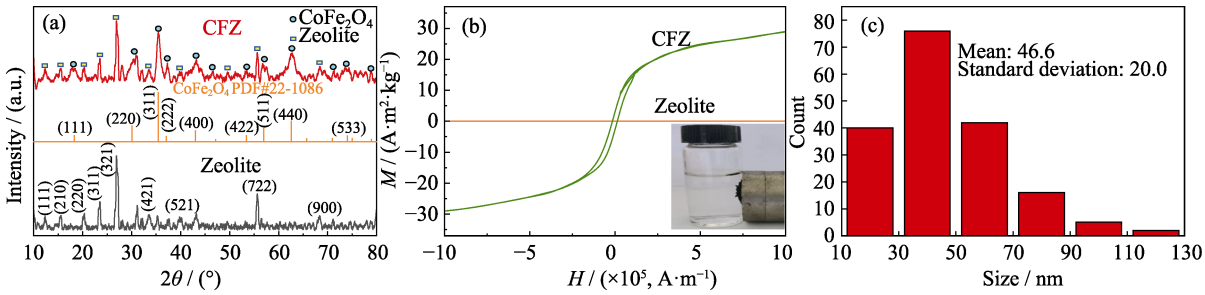

Fig. 1　(a) XRD patterns and (b) magnetic hysteresis loops of the zeolite and CFZ, and (c) size distribution of $CoFe_2O_4$ nanoparticles

value is lower than pure $CoFe_2O_4$ (51.8 $A{\cdot}m^2{\cdot}kg^{-1}$)[18], it is adequate for effective magnetic separation. As shown in the inset of Fig. 1(b), more than 99.5% (mass ratio) of CFZ could be collected by a hand magnet.

The morphology of CFZ was characterized by scanning electron microscope (SEM). As shown in Fig. 2(a), the prepared zeolite with a cuboidal shape is 2–3 μm in diameter, which is the typical shape of Na-A zeolite. The surface of the prepared zeolite is smooth, but its morphology is changed obviously after the modification of $CoFe_2O_4$. As displayed in Fig. 2(b), the zeolite is totally covered and the surface becomes bumpy, but the cube prototype is faintly visible, which suggests that the shell layer is not thick. As shown in Fig. 1(c), size distribution is calculated by ImageJ software, indicating that the shell is composed of 10–130 nm particles, and the mean is around 46.6 nm.

In order to learn about the distribution of elements in CFZ, EDS mapping analyses (Fig. 2(c-f)) were carried out. It can be seen that the content of O, Si and Al elements in CFZ is higher than Fe and Co, and all of them distribute evenly in the catalyst. Transmission electron microscope (TEM) (Fig. 3(a)) and elemental line scanning were selected to investigate its overall structure. Clear difference between the inside and outside of the catalyst is shown in the elemental line scanning spectrum (Fig. 3(b)). O, Si and Al elements mainly exist in the interior, while Fe and Co are in the exterior, clearly showing the core-shell structure of CFZ.

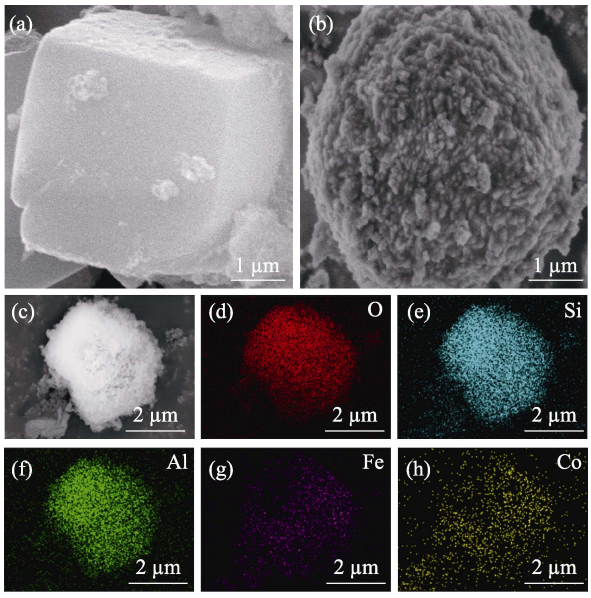

Fig. 2　SEM images of (a) zeolite and (b, c) CFZ, as well as EDS- mappings of (d) O, (e) Si, (f) Al, (g) Fe, and (h) Co

To further figure out the chemical component of CFZ, the surface chemical property was characterized by X-ray photoelectron spectroscope (XPS). The survey spectrum (Fig. 3(c)) clearly shows that Fe, Co, O, Si and Al elements exist in CFZ. As shown in the Fe2p spectrum (Fig. 3(d)), the peaks located at 724.5 and 710.8 eV are ascribed to $Fe2p_{1/2}$ and $Fe2p_{3/2}$, respectively, evidencing the existence of Fe^{3+} and absence of Fe^{2+} on the surface. Fig. 3(e) shows that the Co2p spectrum has two main peaks at around 780.4 and 796.4 eV, associated with the $Co2p_{1/2}$ and $Co2p_{3/2}$, separately. Two corresponding satellite peaks are present at 786.1 and 802.3 eV. It is a solid proof for the presence of Co^{2+} instead of Co^{3+}[19]. The O1s peak is located at 530.6 eV, as illustrated in Fig. 3(f). With Avantage software fitting, it could be divided into two peaks at 530.6 and 532.8 eV, corresponding to the binding energy of lattice oxygen and the oxygen in H_2O, respectively[11, 20]. The lattice oxygen in CFZ may belong to $CoFe_2O_4$, Al_2O_3 and SiO_2. The Fe/Co atomic ratio of CFZ calculated from XPS and element line scanning are 1.93 and 2.07, respectively, which are close to the stoichiometric ratio in $CoFe_2O_4$ molecule. The XPS results clearly verify the formation of $CoFe_2O_4$ on the surface, which gives further proof for the fabrication of magnetic CFZ composite.

N_2 adsorption/desorption isotherms of CFZ and zeolite are shown in Fig. 4(a). It is found that both the zeolite and CFZ have a H3 hysteresis adsorption isotherm, indicating their porous structure[21]. The specific surface area (S_{BET}) of the zeolite is 30.13 m^2/g. Interestingly, the S_{BET} of CFZ is 107.06 m^2/g, more than three times that of zeolite (Table 1). The increase of S_{BET} could be related to the accumulation of nanoparticles in the $CoFe_2O_4$ shell.

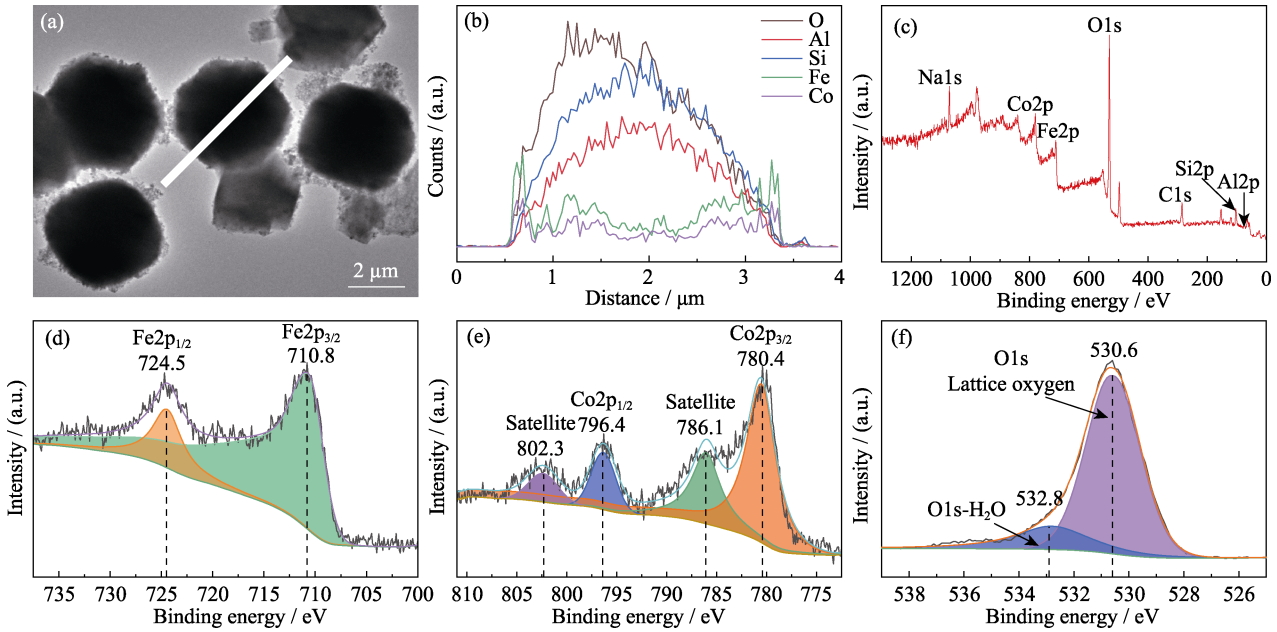

Fig. 3 (a) TEM image and (b) elemental line scanning spectra of CFZ, as well as XPS spectra of (c) survey, (d) Fe2p, (e) Co2p, and (f) O1s of CFZ

Colorful figures are available on website

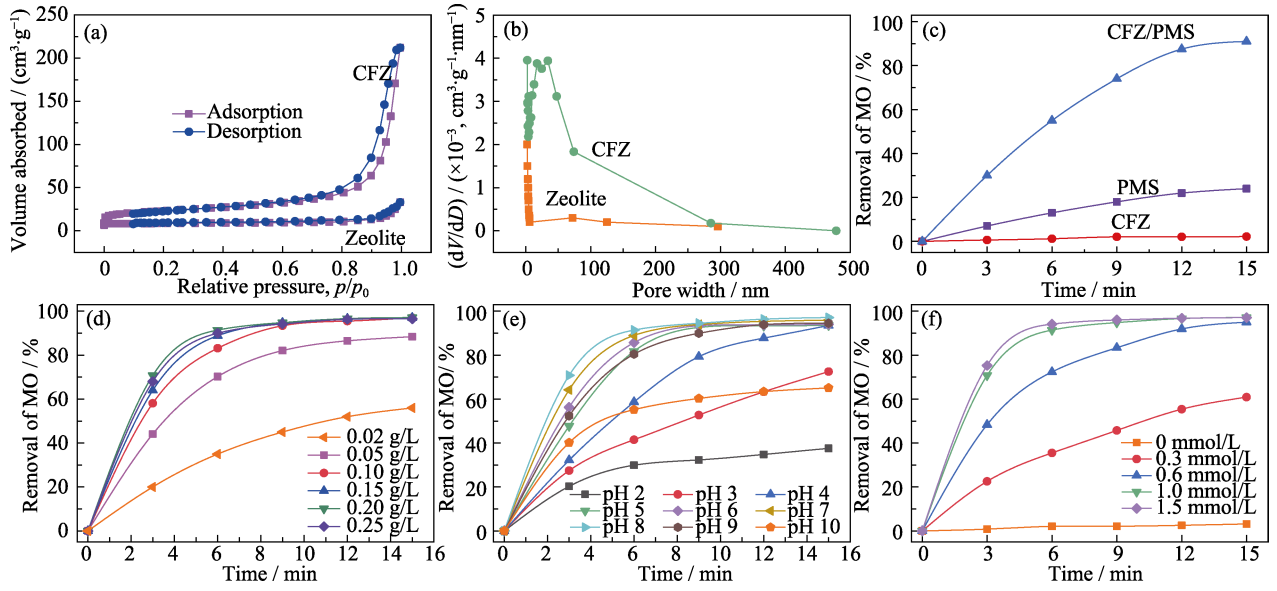

Fig. 4 (a) N_2 adsorption-desorption isotherms and (b) pore size distributions of the prepared zeolite and CFZ, (c) removal of MO in different systems (0.2 g/L CFZ, [PMS] = 0.6 mmol/L, [MO] = 0.2 g/L, pH 8, T = 25 ℃), and effects of (d) catalyst dosage, (e) initial solution pH and (f) PMS concentration on MO removal (0.2 g/L CFZ, [PMS] = 1 mmol/L, [MO] = 50 mg/L, pH 8, T = 25 ℃)

Colorful figures are available on website

As displayed in Fig. 4(b), the pore volumes of micropores, mesopores and macropores all increase obviously, which could come from the shell layer composed of tightly packed nanoparticles. The accumulation of nanoparticles can produce various pores. Owing to the highly porous structure of shell layer, the pore structure of the zeolite is still able to be fully utilized. The increase of S_{BET} would be beneficial to surface adsorption and catalytic degradation of organic pollutant.

Table 1 S_{BET} and pore size analysis data of the prepared zeolite and CFZ

Sample	S_{BET}/($m^2 \cdot g^{-1}$)	Pore volume/ ($cm^3 \cdot g^{-1}$)	Pore size/nm
Zeolite	30.13	0.08	15.00
CFZ	107.06	0.33	16.24

2.2 Removal of MO in different systems

The removal of MO in sole-PMS, sole-CFZ and

PMS/CFZ systems was determined and compared. As shown in Fig. 4(c), the removal rates of MO in the sole-PMS and sole-CFZ system were 23.9% and 3.5%, respectively, after 15 min reaction. While in the CFZ/PMS system, the removal rate increased significantly. The removal rate reached 91.3%, which was more than 3.8 times of that using PMS alone. The removal by sole-CFZ could be attributed to adsorption by the porous $CoFe_2O_4$ shell. Obviously, compared with the total removal, the adsorption is only a small amount. The low adsorption might be owing to the small dosage and short adsorption time. The removal of MO in sole-PMS system could be in a non-radical way as the degradation of sulfachloropyridazine, moxifloxacin and sulfonamides[15, 22-23]. The degradation rate and utilization of oxidant were relatively low. The significant enhancement of removal efficiency in the CFZ/PMS system suggests that the degradation mechanism change a lot in the presence of CFZ. As the previous studies on the catalytic process of PMS oxidation, ROS could play an important role[11]. The production of ROS is determined by the structure and property of the catalyst. Therefore, the high removal rate of the CFZ/PMS system could be related to the synergistic action between CFZ and PMS, which generated a tremendous amount of ROS[23-26].

2.3 Influence of major factors on the degradation

The effect of catalyst dose in the range of 0.02–0.25 g/L on the degradation was studied in the CFZ/PMS system. As shown in Fig. 4(d), even if only 0.02 g/L CFZ was added, the degradation rate could be twice that of sole-PMS. The MO removal increased from 55.9% to 97.1% with the increase of the CFZ dosage from 0.02 to 0.20 g/L. The enhancement of the degradation might be ascribed to an increase in active catalytic sites, which accelerated the conversion reaction between PMS and ROS. Hence, more ROS were generated, such as $O_2^{\bullet-}$ and $^1O_2$[27]. However, when the dosage exceeded 0.20 g/L, the removal of MO did not increase continuously, suggesting there is an optimal ratio between CFZ and PMS. When the CFZ dosage exceeded this value, the available PMS was not adequate so as not to produce more ROS[28]. Considering the balance between catalytic performance and the cost, 0.20 g/L was chosen as the optimal dosage.

In order to detect the influence of initial solution pH on the catalytic activity of CFZ, the degradation at initial solution pH 2–9 was investigated. As shown in Fig. 4(e), in the range of pH 5–9, the MO removal all reached 97% after around 15 min. Since the CFZ catalyst has good catalytic activity in a wide pH range, it is quite potential in practical application for industrial sewage treatment. However, the catalytic activity decreased fast with the increase of acidity as initial solution pH<5. The removal efficiency reduced to 37.6%, when pH decreased to 2. The decrease of catalytic activity could be owing to the enhanced stability of PMS molecules under low initial solution pH condition, which hindered the production of ROS and lowered its catalytic activity[7]. Besides, the high concentration of H^+ could capture the generated ROS, *e.g*. $SO_4^{\bullet-}$ and •OH (Eq. (2, 3))[29-30]. It was also reported that the formation of H–bond between H^+ and the O–O groups of HSO_5^- in acidic pH could hinder the interaction between HSO_5^- and positively charged catalyst surface[31]. Interestingly, the MO degradation also declined under strong alkaline condition. The removal efficiency decreased to 65.1% at pH 10. The reason is probably due to that the CFZ catalyst is negatively charged and repulsive to both HSO_5^- and SO_5^{2-}[28].

$$H^+ + e^- + \bullet OH \rightarrow H_2O \quad (2)$$

$$H^+ + e^- + SO_4^{\bullet-} \rightarrow HSO_4^{\bullet-} \quad (3)$$

PMS dosage also has significant effect on the MO degradation. As exhibited in Fig. 4(f), when the PMS dosage increased from 0.3 to 1.0 mmol/L, the removal efficiency raised from 60.9% to 97.1%, respectively, suggesting that a certain concentration of PMS is necessary to produce high concentration of ROS in the presence of CFZ catalyst. The more PMS, the faster ROS would be produced, unless all the full catalytic activity of CFZ was excited. Further adding PMS did not improve the removal efficiency. Furthermore, excessive PMS dosage in reaction system would reduce the amount of ROS by the ego depletion as well[29, 32-33]. As shown in Fig. 4(f), the removal rate at 1.5 mmol/L PMS addition was not higher than that at 1.0 mmol/L addition. Therefore, the optimal dosage of PMS was about 1.0 mmol/L.

Actual industrial wastewater usually contains various inorganic ions, which may significantly impact the degradation reaction. Herein, SO_4^{2-}, Cl^-, $H_2PO_4^-$ and CO_3^{2-} with a concentration of 50 mg/L were selected to explore their influence on the catalytic activity of CFZ. As shown in Fig. 5(a), the removal efficiency decreased to 95.6%, 95.3%, 95.1% and 90.5% in the presence of SO_4^{2-}, Cl^-, $H_2PO_4^-$ and CO_3^{2-}, respectively. The inhibition was ranked as $CO_3^{2-} > H_2PO_4^- > Cl^- > SO_4^{2-}$. Only CO_3^{2-} caused a slightly larger effect on the catalytic performance. The effect of CO_3^{2-} could be owing to its reaction with ROS, consuming part of •OH, $SO_4^{\bullet-}$ and HSO_5^- to generate some free radicals with low redox potential (Eq. (4, 5))[13, 28, 34]. As shown in Fig. S2, when the concentration of coexisting anions increased to 1000 mg/L, the removal efficiency still achieved 90.7%. It turned out that the influence of most coexisting anions on the catalytic degradation was quite limited, thus the CFZ catalyst could be applied in high salinity industrial wastewater.

$$CO_3^{2-} + SO_4^{\bullet-} \rightarrow SO_4^{2-} + CO_3^{\bullet-} \quad (4)$$

$$CO_3^{2-} + \bullet OH \rightarrow CO_3^{\bullet-} + OH^- \quad (5)$$

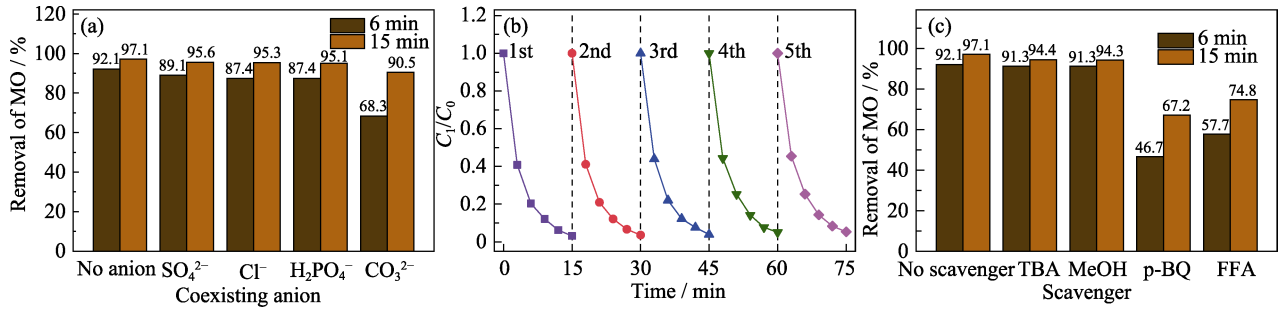

Fig. 5 Effects of (a) coexisting anions on MO removal, (b) cyclic experiments and (c) ROS quenching tests (0.2 g/L CFZ, under the conditions of [PMS] = 1 mmol/L, [MO] = [coexisting anions] = 50 mg/L, pH 8, T = 25 ℃, [scavengers] = 100 mmol/L)
Colorful figures are available on website

2.4 Reusability and stability evaluation of CFZ

To verify the continuous catalytic activity of CFZ, it was recycled for 5 times to estimate its recyclability. As revealed in Fig. 5(b), the removal efficiency of MO still remained 94.7% after 5 cycles. The slight decline (2.4%) of the removal efficiency could be attributed to the deactivation of reactive sites resulted from minor amount of leached Co and Fe from CFZ. Serious measurement found that 0.09 mg/L cobalt ions was released from CFZ in the examined reaction time (15 min), which could meet the emission standard (<1 mg/L). To further prove its stability, XRD and SEM were used to characterize the catalyst cycled for 5 times. As shown in Fig. S3, compared with the fresh catalyst, the XRD pattern of the used sample had little change and no new diffraction peak presented. SEM images (Fig. S4) indicate that most of the CFZ particles preserved the original morphology and structure. The cyclic test and discussion above suggest that CFZ has excellent reusability and stability.

2.5 Catalytic mechanism of CFZ

2.5.1 Determination of ROS

It was reported that $SO_4^{\bullet-}$, •OH, $O_2^{\bullet-}$ and $^1O_2$ play an important role in the process of PMS activation. To figure out the existence of ROS and their contribution to the degradation, methanol (MeOH), tert-butanol (TBA), *p*-benzoquinone (*p*-BQ) and furfuryl alcohol (FFA) were used as scavengers to rapidly quench $SO_4^{\bullet-}$, •OH, $O_2^{\bullet-}$ and $^1O_2$, respectively. As illustrated in Fig. 5(c), the removal efficiency declined from 97.1% to 94.4%, 94.3%, 67.2% and 74.8% with the addition of MeOH, TBA, *p*-BQ and FFA, separately. It is suggested that *p*-BQ and FFA inhibit the degradation significantly, while MeOH and TBA only have a slight impact. The result implies that $O_2^{\bullet-}$ and $^1O_2$ could play a predominant role in the catalytic oxidation.

2.5.2 Mechanism of catalytic oxidation

According to the discussion above, it could be derived that CFZ could activate PMS to selectively generate $O_2^{\bullet-}$ and $^1O_2$ (Fig. 6). The generation of $^1O_2$ from PMS was reported previously and applied in degrading *p*-chlorophenol and sulfamethoxazole[35-36]. $^1O_2$ could be produced by several pathways, as described in Eq. (6-14). $O_2^{\bullet-}$ might be produced by the hydrolysis of PMS (Eq. (9)), and there is no extra side reaction. As shown in Eq. (6-8, 11), $O_2^{\bullet-}$ could also be the precursor to produce $^1O_2$[11, 37]. In this reaction, •OH would also be produced at the same time. Since little •OH was tested by the scavenger experiment, the reaction of Eq. (7, 8, 11) could be ruled out. As a result, the high concentration of $^1O_2$ could be generated from the reaction among HSO_5^-, SO_5^{2-}, $SO_5^{\bullet-}$ and H_2O (Eq. (10, 12-14))[11, 37-40]. To sum up, the excellent catalytic performance of CFZ should be closely related to its promotion in the reaction that produces $O_2^{\bullet-}$ and $^1O_2$. In the CFZ/PMS system, part of these reactions were catalyzed and enhanced by the synergistic interaction between Fe, Co and PMS[7]. As a result, tremendous amount of $^1O_2$ and $O_2^{\bullet-}$ were employed to react with MO. Since the oxidation of $^1O_2$ and $O_2^{\bullet-}$ is quite strong, MO was decomposed efficiently.

$$HSO_5^- \rightarrow SO_5^{2-} + H^+ \quad (6)$$

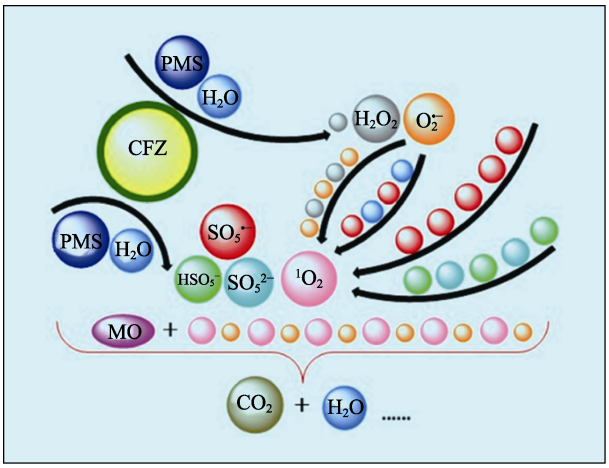

Fig. 6 Schematic of ROS generation and MO degradation
The black arrows show the generation route of ROS and the balls with colors correspond to different reactants, intermediates or products
Colorful figures are available on website

$$SO_5^{2-} + H_2O \rightarrow H_2O_2 + SO_4^{2-} \quad (7)$$

$$HSO_5^- + H_2O \rightarrow H_2O_2 + HSO_4^- \quad (8)$$

$$3HSO_5^- + H_2O \rightarrow 3SO_4^{2-} + 2O_2^{\bullet-} \quad (9)$$

$$HSO_5^- + SO_5^{2-} \rightarrow HSO_4^- + SO_4^{2-} + {}^1O_2 \quad (10)$$

$$O_2^{\bullet-} + H_2O_2 \rightarrow {\bullet}OH + OH^- + {}^1O_2 \quad (11)$$

$$HSO_5^- \rightarrow SO_5^{\bullet-} + H^+ + e^- \quad (12)$$

$$SO_5^{\bullet-} + SO_5^{\bullet-} \rightarrow S_2O_8^{2-}/2SO_4^{2-} + {}^1O_2 \quad (13)$$

$$SO_5^{\bullet-} + H_2O \rightarrow 2HSO_4^- + 1.5{}^1O_2 \quad (14)$$

3 Conclusions

In this study, magnetic CFZ catalyst with high catalytic activity was synthesized *via* the co-precipitation hydrothermal method, and exploited as a PMS activator to degrade MO. Careful investigations indicated that highly porous layer composed of nano-sized $CoFe_2O_4$ particles was covered on the prepared Na-A zeolite. Compared to sole-PMS and sole-CFZ, the CFZ/PMS system exhibited much better catalytic performance. The MO degradation efficiency achieved 97.1% under the optimum reaction condition ([MO]=50 mg/L, [PMS]=1 mmol/L, 0.2 g/L CFZ, pH 8 and T=25 ℃). Except CO_3^{2-}, coexisting anions ($H_2PO_4^-$, Cl^- and SO_4^{2-}) have slight impact on the degradation, suggesting that the CFZ/PMS system has the potential to be used in high salinity wastewater treatment. With efficient magnetic separation technology, the used CFZ is easy to be recycled. After 5 cycles, the MO degradation rate is still achieved 94.7%. The ROS quenching tests suggest that $^1O_2$ and $O_2^{\bullet-}$ play a main role in the degradation.

Supporting materials:

Supporting materials related to this article can be found at https://doi.org/10.15541/jim20220591.

References:

[1] LYU W, LI J, TRCHOVA M, *et al.* Fabrication of polyaniline/poly (vinyl alcohol)/montmorillonite hybrid aerogels toward efficient adsorption of organic dye pollutants. *J. Hazard Mater.*, 2022, **435:** 129004.

[2] SUN B, YUAN Y, LI H, *et al.* Waste-cellulose-derived porous carbon adsorbents for methyl orange removal. *Chem. Eng. J.*, 2019, **371:** 55.

[3] ZHANG S, LIU Y, MA R, *et al.* Molybdenum (VI)-oxo clusters incorporation activates g-C_3N_4 with simultaneously regulating charge transfer and reaction centers for boosting photocatalytic performance. *Adv. Fun. Mater.*, 2022, **32(38):** 2204175.

[4] ISSAKA E, AMU-DARKO J N, YAKUBU S, *et al.* Advanced catalytic ozonation for degradation of pharmaceutical pollutants-a review. *Chemosphere*, 2022, **289:** 133208.

[5] LIU B, JI J, ZHANG B, *et al.* Catalytic ozonation of VOCs at low temperature: a comprehensive review. *J. Hazard Mater.*, 2022, **422:** 126847.

[6] OYEKUNLE D T, GENDY E A, IFTHIKAR J, *et al.* Heterogeneous activation of persulfate by metal and non-metal catalyst for the degradation of sulfamethoxazole: a review. *Chem. Eng. J.*, 2022, **437:** 135277.

[7] PENG Y, TANG H, YAO B, *et al.* Activation of peroxymonosulfate (PMS) by spinel ferrite and their composites in degradation of organic pollutants: a review. *Chem. Eng. J.*, 2021, **414:** 128800.

[8] ZHANG S, LIU Y, GU P, *et al.* Enhanced photodegradation of toxic organic pollutants using dual-oxygen-doped porous g-C_3N_4: mechanism exploration from both experimental and DFT studies. *Appl.Catal. B: Environ.*, 2019, **248:** 1.

[9] ZHANG S, SONG S, GU P, *et al.* Visible-light-driven activation of persulfate over cyano and hydroxyl group co-modified mesoporous g-C_3N_4 for boosting Bisphenol A degradation. *J. Mater. Chem. A*, 2019, **7(10):** 5552.

[10] PARK J, CHOE J K, LEE W, *et al.* Highly fast and selective removal of nitrate in groundwater by bimetallic catalysts supported by fly ash-derived zeolite Na-X. *Environ. Sci.: Nano*, 2020, **7(11):** 3360.

[11] LI J, GOU G, ZHAO H, *et al.* Efficient peroxymonosulfate activation by $CoFe_2O_4$-CeO_2 composite: performance and catalytic mechanism. *Chem. Eng. J.*, 2022, **435:** 134840.

[12] BALAKRISHNAN R M, ILANGO I, GAMANA G, *et al.* Cobalt ferrite nanoparticles and peroxymonosulfate system for the removal of ampicillin from aqueous solution. *J. Water Proc. Eng.*, 2021, **40:** 101823.

[13] GHANBARI F, MORADI M. Application of peroxymonosulfate and its activation methods for degradation of environmental organic pollutants: review. *Chem. Eng. J.*, 2017, **310:** 41.

[14] ZHENG X, NIU X, ZHANG D, *et al.* Metal-based catalysts for persulfate and peroxymonosulfate activation in heterogeneous ways: a review. *Chem. Eng. J.*, 2022, **429:** 132323.

[15] WANG Q, SHAO Y, GAO N, *et al.* Activation of peroxymonosulfate by Al_2O_3-based $CoFe_2O_4$ for the degradation of sulfachloropyridazine sodium: kinetics and mechanism. *Separ. and Purif. Tech.*, 2017, **189:** 176.

[16] KEFENI K K, MAMBA B B. Photocatalytic application of spinel ferrite nanoparticles and nanocomposites in wastewater treatment: review. *Sustain. Mater. Tech.*, 2020, **23:** e00140.

[17] SONG L, LI J, ZHANG Z, *et al.* La-containing magnetic zeolite synthesized from gangue by ball-milling method. *Mater. Lett.*, 2021, **303:** 130542.

[18] MARTINEZ-VARGAS S, MARTÍNEZ A I, HERNÁNDEZ-BETETA E E, *et al.* Arsenic adsorption on cobalt and manganese ferrite nanoparticles. *J. Mater. Sci.*, 2017, **52(11):** 6205.

[19] CHAGAS C A, DE SOUZA E F, DE CARVALHO M C N A, *et al.* Cobalt ferrite nanoparticles for the preferential oxidation of CO. *Appl. Catal. A: Gener.*, 2016, **519:** 139.

[20] LIU Z, GAO Z, WU Q. Activation of persulfate by magnetic zirconium-doped manganese ferrite for efficient degradation of tetracycline. *Chem. Eng. J.*, 2021, **423:** 130283.

[21] PENIDO E S, MELO L C A, GUILHERME L R G, *et al.* Cadmium binding mechanisms and adsorption capacity by novel phosphorus/magnesium-engineered biochars. *Science of The Total Environment*, 2019, **671:** 1134.

[22] JI Y, LU J, WANG L, *et al.* Non-activated peroxymonosulfate oxidation of sulfonamide antibiotics in water: kinetics, mechanisms, and implications for water treatment. *Water Res.*, 2018, **147:** 82.

[23] LIU L, MI H, ZHANG M, *et al.* Efficient moxifloxacin degradation by $CoFe_2O_4$ magnetic nanoparticles activated peroxymonosulfate: kinetics, pathways and mechanisms. *Chem. Eng. J.*, 2021, **407:** 127201.

[24] CHEN L, DING D, LIU C, *et al.* Degradation of norfloxacin by

$CoFe_2O_4$-GO composite coupled with peroxymonosulfate: a comparative study and mechanistic consideration. *Chem. Eng. J.*, 2018, **334:** 273.

[25] DU Y, MA W, LIU P, *et al.* Magnetic $CoFe_2O_4$ nanoparticles supported on titanate nanotubes ($CoFe_2O_4$/TNTs) as a novel heterogeneous catalyst for peroxymonosulfate activation and degradation of organic pollutants. *J. Hazard Mater.*, 2016, **308:** 58.

[26] HUNG C M, CHEN C W, HUANG C P, *et al.* Removal of 4-nonylphenol in activated sludge by peroxymonosulfate activated with sorghum distillery residue-derived biochar. *Bioresour Technol.*, 2022, **360:** 127564.

[27] DUNG N T, TRANG T T, THAO V D, *et al.* Enhanced degradation of organic dyes by peroxymonosulfate with Fe_3O_4-$CoCO_3$/rGO hybrid activation: a comprehensive study. *J. the Taiwan Instit. of Chem. Engin.*, 2022, **133:** 104279.

[28] DUNG N T, THU T V, VAN NGUYEN T, *et al.* Catalytic activation of peroxymonosulfate with manganese cobaltite nanoparticles for the degradation of organic dyes. *RSC Adv.*, 2020, **10(7):** 3775.

[29] CHEN G, NENGZI L C, GAO Y, *et al.* Degradation of tartrazine by peroxymonosulfate through magnetic Fe_2O_3/Mn_2O_3 composites activation. *Chine. Chemi. Lett.*, 2020, **31(10):** 2730.

[30] XU P, XIE S, LIU X, *et al.* Electrochemical enhanced heterogenous activation of peroxymonosulfate using $CuFe_2O_4$ particle electrodes for the degradation of diclofenac. *Chem. Eng. J.*, 2022, **446:** 136941.

[31] ZHANG T, ZHU H, CROUE J P. Production of sulfate radical from peroxymonosulfate induced by a magnetically separable $CuFe_2O_4$ spinel in water: efficiency, stability, and mechanism. *Environ. Sci. Technol.*, 2013, **47(6):** 2784.

[32] LI J, WAN Y, LI Y, *et al.* Surface Fe(III)/Fe(II) cycle promoted the degradation of atrazine by peroxymonosulfate activation in the presence of hydroxylamine. *Appl. Catal. B: Environ.*, 2019, **256:** 117782.

[33] WANG Z, NENGZI L C, ZHANG X, *et al.* Novel $NiCo_2S_4$/CS membranes as efficient catalysts for activating persulfate and its high activity for degradation of nimesulide. *Chem. Eng. J.*, 2020, **381:** 122517.

[34] WANG S, CHEN Z, YAN P, *et al.* Enhanced degradation of iohexol in water by $CuFe_2O_4$ activated peroxymonosulfate: efficiency, mechanism and degradation pathway. *Chemosphere*, 2022, **289:** 133198.

[35] ZHANG L S, JIANG X H, ZHONG Z A, *et al.* Carbon nitride supported high-loading Fe single-atom catalyst for activation of peroxymonosulfate to generate $^1O_2$ with 100% selectivity. *Angew. Chem. Int. Ed.*, 2021, **60(40):** 21751.

[36] WANG J, SHEN M, WANG H, *et al.* Red mud modified sludge biochar for the activation of peroxymonosulfate: singlet oxygen dominated mechanism and toxicity prediction. *Sci. Total. Environ.*, 2020, **740:** 140388.

[37] ZHENG Y, ZHUANG W, ZHANG X, *et al.* Grape-like CNTs/$BaTiO_3$ nanocatalyst boosted hydraulic-driven piezo-activation of peroxymonosulfate for carbamazepine removal. *Chem. Eng. J.*, 2022, **449:** 137826.

[38] WANG X, ZHUANG Y, SHI B. Degradation of trichloroacetic acid by MOFs-templated CoFe/graphene aerogels in peroxymonosulfate activation. *Chem. Eng. J.*, 2022, **450:** 137799.

[39] XU A, WU D, ZHANG R, *et al.* Bio-synthesis of Co-doped $FeMnO_x$ and its efficient activation of peroxymonosulfate for the degradation of moxifloxacin. *Chem. Eng. J.*, 2022, **435:** 134695.

[40] ZHAO Y, WANG H, JI J, *et al.* Degradation of ciprofloxacin by peroxymonosulfate activation using catalyst derived from spent lithium-ion batteries. *J. Cleaner Produc.*, 2022, **362:** 132442.

$CoFe_2O_4$@Zeolite 催化剂活化过一硫酸盐对甲基橙的强化降解: 性能与机理

王 磊[1], 李建军[1,2], 宁 军[3], 胡天玉[1,2], 王洪阳[1], 张占群[1], 武琳馨[1]

(1. 安徽理工大学 材料科学与工程学院, 淮南 232001; 2. 安徽理工大学 环境友好材料与职业健康研究院, 芜湖 241000; 3. 安徽水韵环保股份有限公司, 芜湖 241000)

摘 要: 采用共沉淀水热法制备了 $CoFe_2O_4$@Zeolite (CFZ), 并将其用于活化过一硫酸盐(PMS)降解合成染料。综合表征表明, 组成多孔壳层的 $CoFe_2O_4$ 纳米颗粒均匀地覆盖在 Na-A 沸石上。CFZ 的比表面积为 107.06 m^2/g, 是原始沸石比表面积的 3 倍。CFZ 的饱和磁化强度为 29.0 $A·m^2·kg^{-1}$, 可以进行有效磁分离。催化降解实验表明, CFZ/PMS 体系对甲基橙(MO)的去除率远远高于单独使用 CFZ 或 PMS。在最佳条件([MO]=50 mg/L、[PMS]=1.0 mmol/L、0.2 g/L CFZ、pH 8 和 *T*=25 ℃)下, MO 去除率可达到 97.1%。实验研究了 pH、PMS 用量、CFZ 用量、MO 浓度以及共存阴离子等因素对 CFZ 催化性能的影响。活性氧粒子淬灭实验表明, $^1O_2$ 和 $O_2^{\bullet-}$在降解过程中起主导作用。CFZ 具有良好的回收性能, 5 次循环后 MO 去除效率仅下降 2.4%。本文还详细讨论了 CFZ/PMS 体系的催化降解机理。

关 键 词: 高级氧化技术; 过一硫酸盐活化; 磁性催化剂; $CoFe_2O_4$@ Zeolite; 活性氧粒子; 降解

中图分类号: TB332 **文献标志码:** A

Supporting Materials

Enhanced Degradation of Methyl Orange with $CoFe_2O_4$@Zeolite Catalyst as Peroxymonosulfate Activator: Performance and Mechanism

WANG Lei[1], LI Jianjun[1,2], NING Jun[3], HU Tianyu[1,2], WANG Hongyang[1], ZHANG Zhanqun[1], WU Linxin[1]

(1. School of Materials Science and Engineering, Anhui University of Science and Technology, Huainan 232001, China; 2. Institute of Environment-friendly Materials and Occupational Health, Anhui University of Science and Technology, Wuhu 241000, China; 3. Anhui Shuiyun Environmental Protection Co., Ltd., Wuhu 241000, China)

Reagents: PMS ($KHSO_5{\cdot}0.5KHSO_4{\cdot}0.5K_2SO_4$, $KHSO_5$), MO, cobalt chloride ($CoCl_2{\cdot}6H_2O$), ferric chloride ($FeCl_3{\cdot}6H_2O$), sodium metasilicate nonahydrate ($Na_2SiO_3{\cdot}9H_2O$), methanol (MeOH), tert-butyl alcohol (TBA), *p*-Benzoquinone (*p*-BQ), furfuryl alcohol (FFA), sodium carbonate (Na_2CO_3), sodium sulfate (Na_2SO_4), sodium chloride (NaCl) and potassium phosphate monobasic (KH_2PO_4) were purchased from Aladdin Reagent Co., Ltd (Shanghai, China). Coal gangue were collected from Huainan, China. All chemicals above are analytical grade, and deionized water was used throughout all experiments.

Relationship between the concentration and absorbance: Before the degradation experiment, MO solutions with concentration of 0, 2, 4, 6, 8 and 10 mg/L were prepared. The absorbance was measured by ultraviolet-visible spectrophotometer (UV-5100, China) at 464 nm. After linear fitting of MO concentration and absorbance, a functional relationship can be obtained:

$$Y = 0.08194X + 0.04362,\ R^2 = 0.9999 \qquad (1)$$

Where, X and Y are the concentration and absorbance of MO, respectively. It can be seen from the value of R^2 that there is a good linear relationship between the concentration and absorbance of MO.

Characterization methods: The fresh CFZ were investigated by XRD, Smartlab SE, Japan). Brunauer-Emmett-Teller (BET, V-sorb2800p, China) was used to measure the N_2 adsorption-desorption isotherms, and the specific surface area were calculated based on the BET model. The surface morphology, elements distribution and overall structure of CFZ were characterized by Scanning electron microscope (SEM, ZEISS-G500, Germany) equipped with an energy dispersive spectrometer (EDS) and transmission electron microscope (TEM, Tecnai G2 F20, Netherlands). The chemical states of Fe, Co, O were studied by X-ray photoelectron spectroscope (XPS, ESCALAB 250Xi, USA). The saturation magnetization was measured by vibrating sample magnetometer (VSM, HH-20, China) at room temperature. The leached cobalt ions concentration was determined by an inductively coupled plasma mass spectrometry (ICP-MS, Agilent 7700x, USA).

The degradation performance of the CFZ/PMS system at various MO concentrations was also investigated. As shown in Fig. S1, with the increase of MO concentration from 20 to 200 mg/L, the removal efficiency decreased from 98.1% to 92.0%, respectively. It turned out that the CFZ/PMS system has excellent degradation for both low and high concentration dyes, which is of great significance for its practical application.

Treatment of the SO_4^{2-} product during degradation: It was reported that ettringite precipitation is an effective method for handling high-concentration SO_4^{2-}. In the approach, lime and aluminum salts are added into the sewage in turn to react with SO_4^{2-} to form insoluble

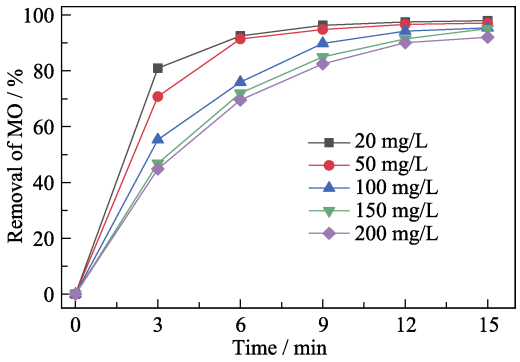

Fig. S1　Degradation performance on different concentrations of MO (0.2 g/L CFZ, [PMS]=1 mmol/L, pH 8, *T*=25 ℃)

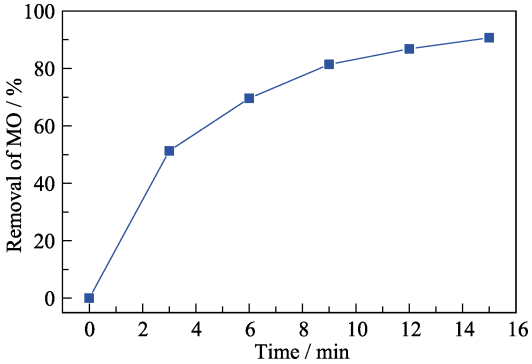

Fig. S2　Effect of high-concentration coexisting anions ([MO]=50 mg/L, $[SO_4^{2-}]$=$[CO_3^{2-}]$=$[Cl^-]$=$[H_2PO_4^{2-}]$=1000 mg/L, 0.2 g/L CFZ, [PMS]=1 mmol/L, pH 7, *T*=25 ℃)

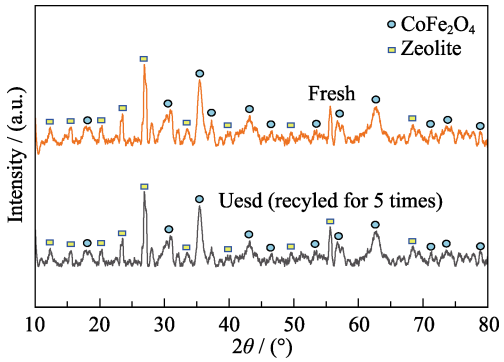

Fig. S3 XRD patterns of the fresh CFZ and the used CFZ

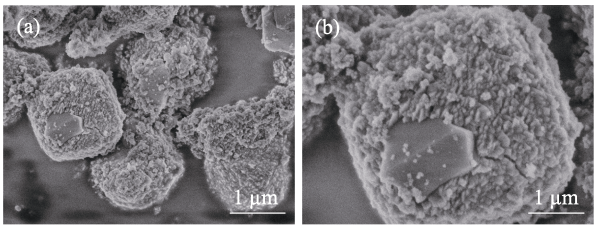

Fig. S4 SEM image of the CFZ cycled for 5 times

ettringite ($Ca_6Al_2(OH)_{12}(SO_4)_3{\cdot}26H_2O$) that can be used as a cement grouting material[S1]. Owing to its high removal efficiency and cost-effectiveness, relative researches have employed this method to deal with industrial sewage, such as textile industries and mine water[S2-S3].

Degradation of methylene blue (MB)

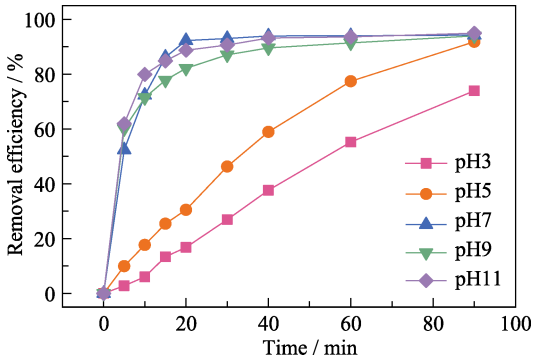

Fig. S5 Effect of initial solution pH on MB removal

Table S1 Removal efficiency of MB under different pH conditions

pH	3	5	7	9	11
Removal efficiency/%	73.96	91.83	94.22	93.99	94.96

References:

[S1] FANG P, TANG Z J, CHEN X B, *et al*. Removal of high-concentration sulfate ions from the sodium alkali FGD wastewater using ettringite precipitation method: factor assessment, feasibility, and prospect. *Journal of Chemistry*, 2018, **2018:** 1265168.

[S2] DOU W, ZHOU Z, JIANG L M, *et al*. Sulfate removal from wastewater using ettringite precipitation: magnesium ion inhibition and process optimization. *Journal of Environmental Management*, 2017, **196:** 518.

[S3] TOLONEN E T, HU T, RAMO J, *et al*. The removal of sulphate from mine water by precipitation as ettringite and the utilisation of the precipitate as a sorbent for arsenate removal. *J. Environ. Manage.*, 2016, **181:** 856.